Physica B 464 (2015) 9–16

Contents lists available at ScienceDirect

Physica B

journal homepage: www.elsevier.com/locate/physb

Theoretical study of the new zintl phases compounds K_2ACdSb_2 (A=(Sr, Ba))

Sikander Azam [a], A.H. Reshak [a,b,*]

[a] New Technologies-Research Center, University of West Bohemia, Univerzitni 8, 306 14 Pilsen, Czech republic
[b] Center of Excellence Geopolymer and Green Technology, School of Material Engineering, University Malaysia Perlis, 01007 Kangar, Perlis, Malaysia

ARTICLE INFO

Article history:
Received 17 June 2014
Received in revised form
14 August 2014
Accepted 13 February 2015
Available online 17 February 2015

Keywords:
FPLAPW calculations
Electronic structure
Charge density
Optical properties
DFT

ABSTRACT

The electronic structure and optical properties of $K_2SrCdSb_2$ and $K_2BaCdSb_2$ compounds are computed using the full potential linearized augmented plane wave (FP-LAPW) method as implemented in WIEN2k code. In this perspective, the local density approximation (LDA), generalized gradient approximation (GGA) and Engel and Vosko approximation (EV-GGA) were used for the exchange correlation potential. The calculated band structure shows a direct band gap of about 0.344/0.20 eV (LDA), 0.463/0.285 eV (GGA) and 0.904/0.707 eV (EV-GGA) for $K_2SrCdSb_2$/$K_2BaCdSb_2$ compounds. The part of different bands was scrutinized from total and partial density of states curves. There is strong hybridization between Sr-s and Sr-p states and also between Cd-d and Sb-s states in the valence band. The electronic charge density has also been studied in the (200) crystallographic plane. The K, Sr/Ba, Cd and Sb atoms shows ionic bonding. Besides this, the optical properties, including the dielectric function are obtained and analyzed in details.

1. Introduction

Motivated by the captivating chemistry and physics of numerous based pnictogen based solid-state compounds [1–10], numerous groups are carrying out systematic study of latest ternary and other newly quaternary antimonides, arsenide and bismuthides. The former research have been very gainful and led to the discovery of various novel zintl compounds such as $Ba_2Cd_2As_3$, $Ba_2Cd_2Sb_3$, $Ba_3Cd_2Sb_4$, $A_{21}Cd_4Bi_{18}$, $A_{21}M_4Sb_{18}$, Ba_2ZnPn_2, $A_9M_{4+x}Sb_9$, $A_{11}M_6Sb_{12}$, $A_9M_{4+x}Bi_9$ and $KA_2Cd_2Sb_3$ [11–19]. Praise worthy of exact suggestion here are the couple of compounds Ca_2CdSb_2 and Yb_2CdSb_2, also zintl phases, which regardless of being isoelectronic assume unlike structures: Yb_2CdSb_2 and Ca_2CdSb_2, the first one crystallizes in the non-centro-symmetric with space group Cmc21 and the last one crystallizes in the centro-symmetric whose space group is Pnma [20]. Such structural difference was considered somewhat astonishing; given how secure the ionic radii of likewise coordinated Ca^{2+} and Yb^{2+} and cations are [20]. Even so, both structures are identical (basically poly types), aspect $^2_\infty[CdSb_2]^{4-}$ poly an ionic layers, made of corner-shared $CdSb_4$ tetrahedral, interspaced by Yb^{2+} or Ca^{2+} cations. In 2010, Saparov et al. [21] presented the synthesis of a new-fangled family of zintl phases Na_2ACdSb_2 and K_2ACdSb_2 (A=Ca, Sr, Ba, Eu, Yb). By means of single-crystal and powder X-ray diffraction studies, it was well-known that Na_2ACdSb_2 and K_2ACdSb_2 crystallize with a narrative structure type, largely comparable to the Yb_2CdSb_2 structure [18].

In the current paper we demonstrate the influence of using different exchange and correlation potential and the substitution of Sr by Ba atom on the electronic band structure, density of states, charge density and optical properties of the new zintl phases compounds K_2ACdSb_2 (A=(Sr, Ba)).

2. Methodology

The crystal structure of $K_2SrCdSb_2$ and $K_2BaCdSb_2$ compounds is shown in Fig. 1. We make use of the crystallographic data from the work of Saparov et al. [21]. Both compounds have orthorhombic structure with space group # 26 (Pmc21). The lattice constants for the $K_2SrCdSb_2$ are $a=4.9317(12)$ Å, $b=9.810(2)$ Å and $c=8.191(2)$ Å and for $K_2BaCdSb_2$ are $a=5.0366(8)$ Å, $b=9.8183(15)$ Å and $c=8.4924(13)$ Å. We have optimized the atomic positions by minimization the forces acting on the atoms. From the relaxed geometry the electronic structure, electronic charge density and the optical properties can be determined. The optimized geometry along with the experimental data [21] are listed in Table 1. The electronic structure and optical properties of $K_2SrCdSb_2$ and $K_2BaCdSb_2$ compounds are studied by using the full potential linearized augmented plane wave as implemented in the WIEN2k

* Corresponding author.
E-mail address: maalidph@yahoo.co.uk (A.H. Reshak).

http://dx.doi.org/10.1016/j.physb.2015.02.010
0921-4526/

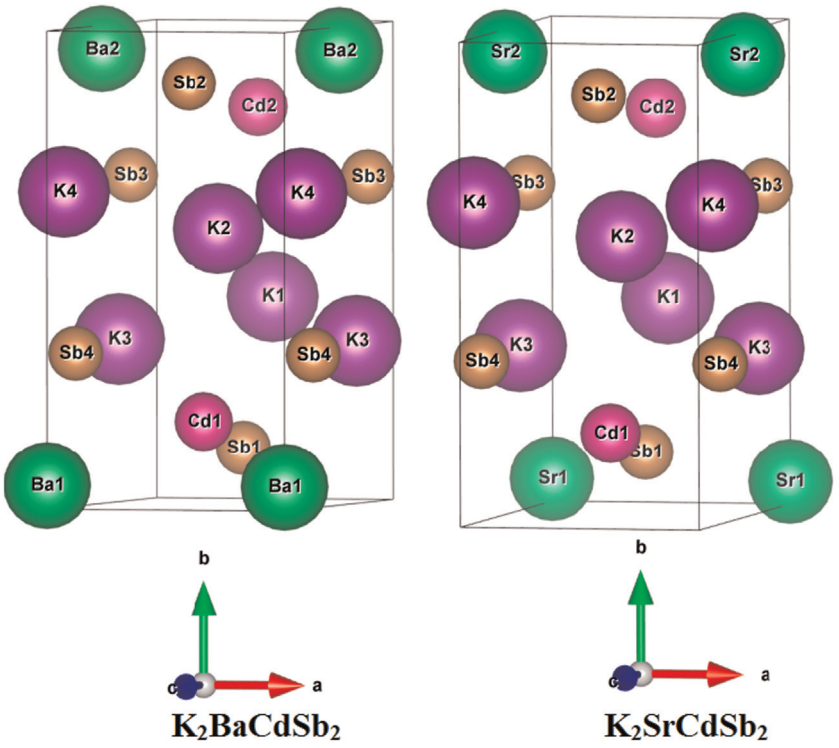

Fig. 1. Unit cell structure for $K_2SrCdSb_2$ and $K_2BaCdSb_2$ compounds.

Table 1
Atomic positions for $K_2SrCdSb_2$ and $K_2BaCdSb_2$ compound.

Atoms	*X* (Exp.)	*X* (Opt.)	*Y* (Exp.)	*Y* (Opt.)	*Z* (Exp.)	*Z* (Opt.)
$K_2SrCdSb_2$						
K1	0.5000	0.5000	0.4236(3)	0.4226	0.0256(3)	0.0339
K2	0.0000	0.0000	0.3391(3)	0.3378	0.3398(3)	0.3496
Sr	0.0000	0.0000	0.0459(1)	0.0455	−0.0030(1)	0.0037
Cd	0.5000	0.5000	0.1758(1)	0.1767	0.6521(1)	0.6591
Sb1	0.5000	0.5000	0.1100(1)	0.1104	0.2831(1)	0.2898
Sb2	0.0000	0.0000	0.6850(1)	0.6836	0.2479(1)	0.2581
$K_2BaCdSb_2$						
K1	0.5000	0.5000	0.4233(2)	0.4231	0.0206(3)	0.0208
K2	0.0000	0.0000	0.3405(2)	0.3400	0.3439(2)	0.3442
Ba	0.0000	0.0000	0.0496(1)	0.0499	0.0000(1)	0.9997
Cd	0.5000	0.5000	0.1769(1)	0.1771	0.6541(1)	0.6539
Sb1	0.5000	0.5000	0.1132(1)	0.1134	0.2888(1)	0.2881
Sb2	0.0000	0.0000	0.6814(1)	0.6803	0.2382(1)	0.2386

code [22]. The perspective is supported by density functional theory (DFT) [23]. The exchange correlation potential was treated via local density approximation (LDA) of Ceperley–Alder, and the generalized gradient approximation (GGA) the scheme of Perdew–Burke–Ernzerhof [24,25], which is based on exchange-correlation energy to calculate the total energy. Also we utilize the Engel–Vosko GGA formalism [26], which optimizes the corresponding potential for band structure calculations. It is well known in the self-consistent band structure calculation within DFT, both LDA and GGA usually underestimate the energy gap [27]. This is mostly due to the fact that they have simple forms that are not adequately flexible to accurately reproduce duplicate both the exchange correlation energy and its ascribe derivative. Engel and Vosko considered this shortcoming and assembled a new functional form of GGA which is adept to better reproduce the exchange potential at the expense of less agreement in the exchange energy. This approach called EV-GGA, yields better band splitting and some other

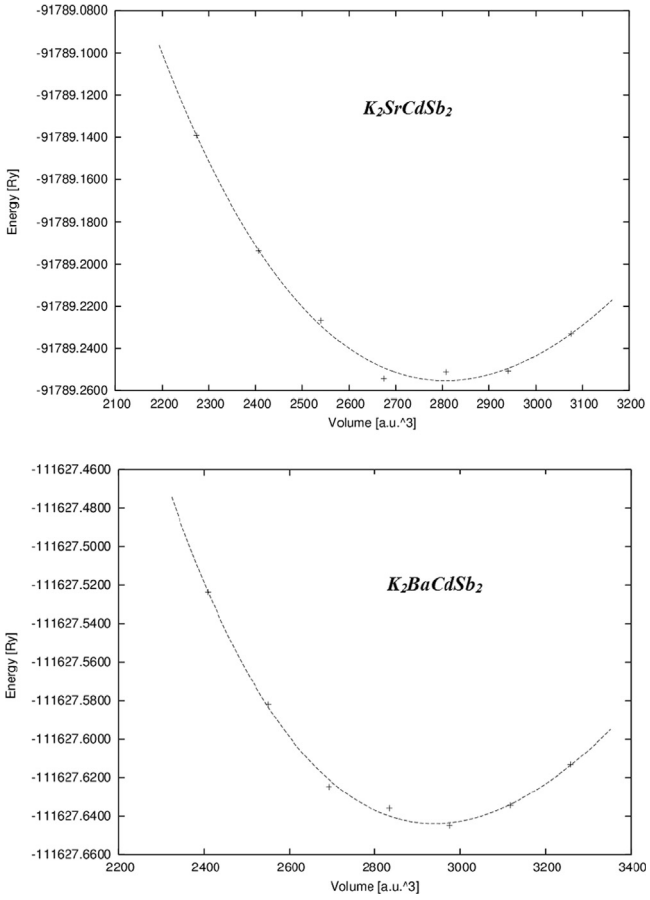

Fig. 2. Variation of total energy (eV) as a function of volume for $K_2SrCdSb_2$ and $K_2BaCdSb_2$ compounds.

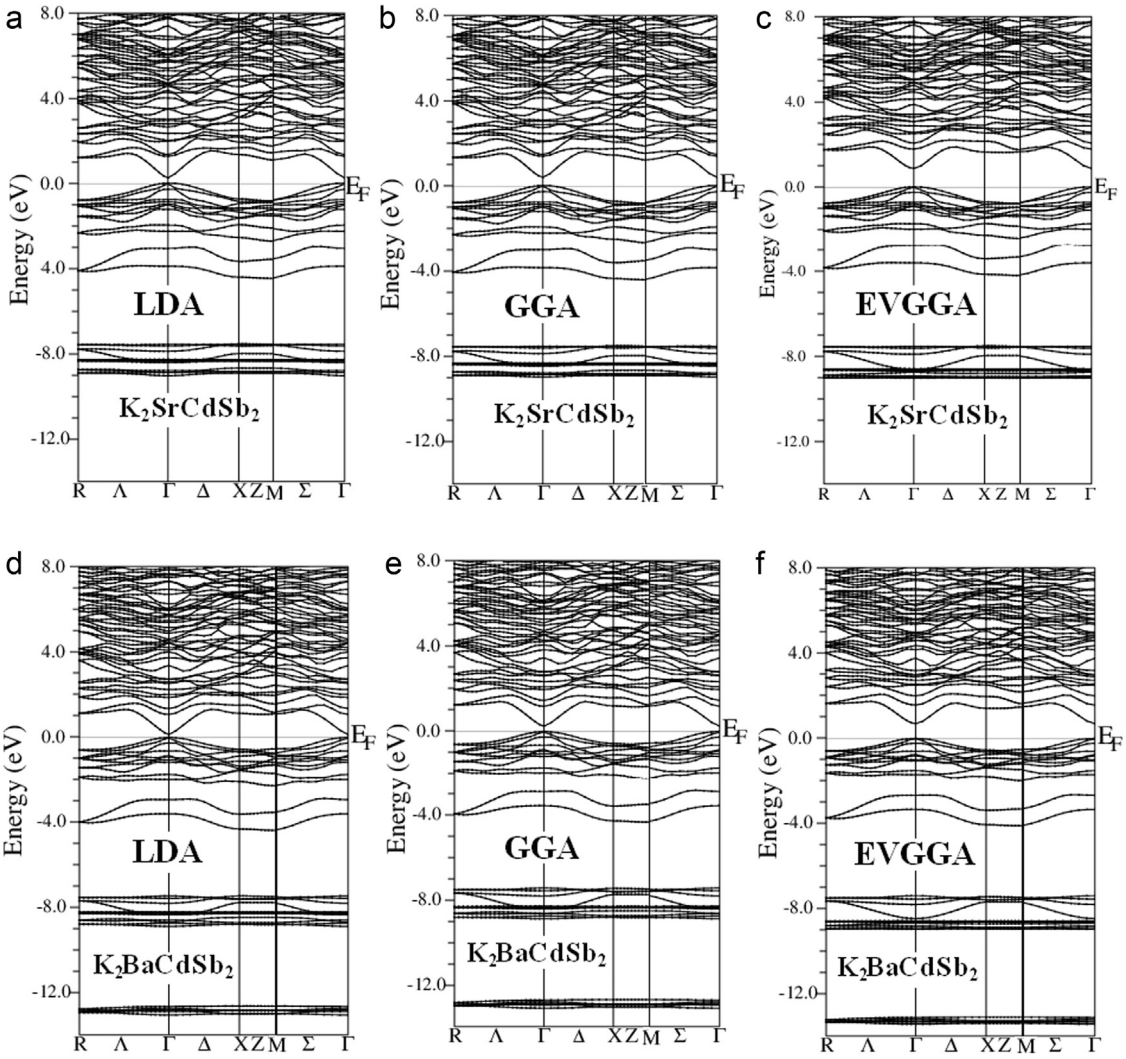

Fig. 3. Calculated total density of state for $K_2SrCdSb_2$ and $K_2BaCdSb_2$ compounds (State/eV unit cell).

properties which mainly depend on the accuracy of exchange correlation potential. On the other hand the quantities which depend on an accurate description of E_x, like the equilibrium volume and bulk modulus are in poor agreement with experiment [27]. For structural properties the exchange-correlation potential was calculated utilizing GGA in the pattern proposed by Perdew et al. [25]. For calculating the electronic band structure and optical properties we applied the Engel–Vosko (EV-GGA) scheme [26].

Kohn–Sham wave functions were prolonged in provisions of spherical harmonic function inside the non-overlapping muffin tin (MT) spheres and among Fourier series in the interstitial region. The ι-expansions of the wave functions were conceded out up to $\iota_{max}=10$ within the muffin-tin spheres of radius R_{MT}. For the charge density the Fourier expansion was up to $G_{max=}12$. In the interstitial regions the wave functions were expanded in plane waves with cut off of $K_{MAX}\times R_{MT}=7.0$, in order to attain the convergence for energy eigen values. The value of muffin-tin radii R_{MT} is chosen to be 2.0 a.u for K, Sr/Ba, Cd and Sb. The self-consistency is obtained using a mesh of 4000 $\vec{k}$ points in the irreducible Brillouin zone (IBZ).

For the optical properties, the dielectric function was deliberated in the momentum representation, which necessitates matrix elements of the momentum p among occupied and unoccupied states. Consequently, the components of the imaginary part of the dielectric function, $\varepsilon_2^{ij}(\omega)$ was computed by using the relation taken from Ref. [27];

$$\varepsilon_2^{ij}(\omega)=\frac{4\pi^2e^2}{Vm^2\omega^2}\times\sum_{knn'\sigma}\langle kn\sigma|p_i|kn'\sigma\rangle\langle kn'\sigma|p_j|kn\sigma\rangle\times f_{kn}\left(1-f_{kn'}\right)\times\sigma(E_{kn'}-E_{kn}-\hbar\omega) \quad (1)$$

where e, m, ω and V are the electron charge, mass, frequency of the incoming electromagnetic radiation and the volume of the unit cell respectively, where $(p_x, p_y, p_z)=p$ is the momentum operator, $|kn\sigma\rangle$ the crystal wave function, corresponding to eigen value E_{kn} with crystal momentum k and spin σ. As a final point, f_{kn} is the Fermi distribution function ensures that just transitions from occupied to unoccupied states are count up, and $\sigma(E_{kn'}-E_{kn}-\omega)$ is the requirements for total energy conservation. The real part $\varepsilon_1(\omega)$ can be gained from the imaginary part $\varepsilon_2(\omega)$ using the Kramer's Kronig dispersion relation [28].

$$\varepsilon_1(\omega)=1+\frac{2}{\pi}P\int_0^\infty\frac{\omega'\varepsilon_2(\omega')}{\omega'^2-\omega^2}d\omega' \quad (2)$$

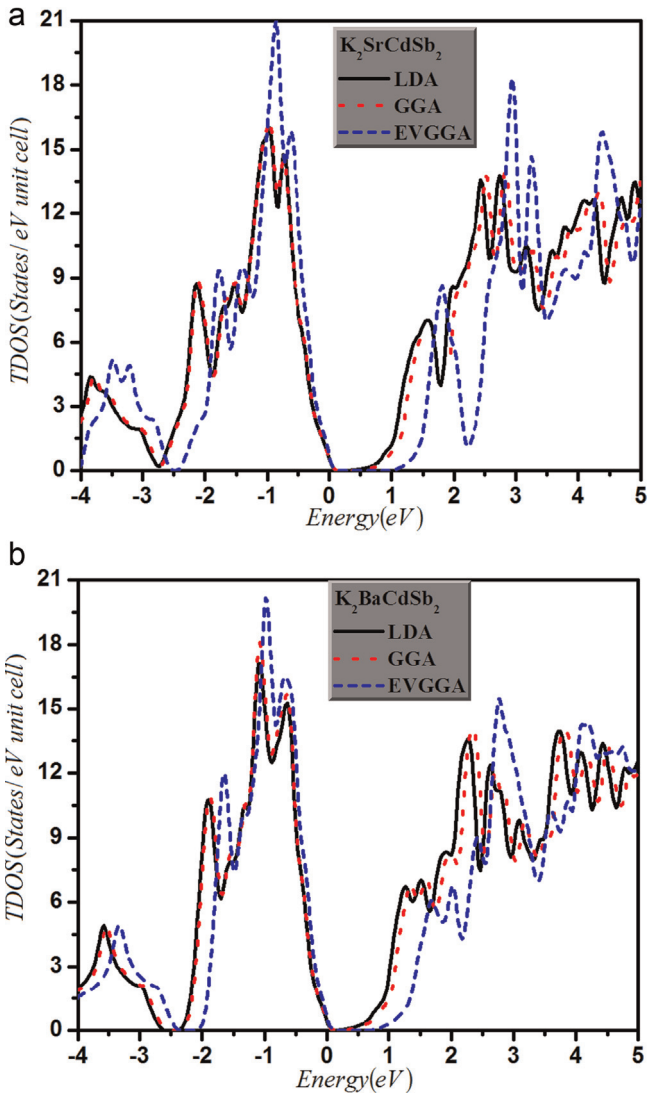

Fig. 4. Calculated partial density of states for $K_2SrCdSb_2$ and $K_2BaCdSb_2$ compounds (States/eV unit cell).

3. Result and discussions

3.1. Structural properties

We have analyzed the structural properties for both compounds; structural optimization was performed by minimizing the total energy with respect to the unit cell volume using the Murnaghan's equation of state (EOS) [29] as shown in Fig. 2. It is obvious from Fig. 2 that the possible stable volume of $K_2SrCdSb_2$ and $K_2BaCdSb_2$ is the one at which the total energy is minimum. From the stable volume we found bulk modulus B(GPa) and pressure derivatives of bulk modulus which are 27.8032 and 2.1283 (29.1017 and 2.8292) for $K_2SrCdSb_2$ ($K_2BaCdSb_2$). The bulk moduli B was calculated using GGA. Fig. 2, show that the compressibility increases as we replace Sr by Ba.

3.2. Band structure and density of states

The electronic band structures of the orthorhombic $K_2SrCdSb_2$ and $K_2BaCdSb_2$ compounds are calculated. In Fig. 3, we show the electronic band dispersion curves along some high symmetry directions of the Brillouin zone of $K_2SrCdSb_2$ and $K_2BaCdSb_2$ compounds for the three approximations. The calculated band structure profiles using the LDA, GGA and EV-GGA are similar excluding the values of their band gaps which were bigger for EV-GGA. Therefore, we will demonstrate only the EVGGA results due to its enhanced band gap. The valence band maximum (VBM) and the conduction band minimum (CBM) are positioned at ε point, resulting in a direct energy band gap of about 0.344/0.20 eV (LDA), 0.463/0.285 eV (GGA) and 0.904/0.707 eV (EV-GGA). It is obvious that the calculated band gaps using EV-GGA are larger than those obtained by LDA and GGA. The calculated electronic structure of $K_2SrCdSb_2$ and $K_2BaCdSb_2$ verifies that the investigated compounds are narrow-gap semiconductors, which is in agreement with the previous work [21]. In order to illuminate the nature of the electronic band structures, we have calculated the total and partial density of states (TDOS and PDOS) for both compounds. These are presented in Figs. 4 and 5. Following these figures, we should stress that there are four distinct structures separated by gaps. The first structure for both compounds at around -15.0 eV, consist entirely of K-p states. The next structure, laying between -9.0 and -7.0 eV for both compounds consist of Cd-d, in addition the $K_2SrCdSb_2$ compound consist of Sr-p. At the energy range between -4.0 and E_F, the $K_2SrCdSb_2$ compound consists entirely of Sr-s/p, Cd-p and Sb-p states, while $K_2BaCdSb_2$ compound consist of Ba-s/d states. The lower conduction bands of $K_2BaCdSb_2$ compound situated in the region between 0.2 eV and 16.0 eV, mainly consist of Sb-d states, whereas for $K_2SrCdSb_2$ compound the energy region from 0.34 eV to 16.0 eV consist of Sb-p and Sr-p/d. From the partial DOS, we noticed that both of Ba and K show minimal contribution to the CBM and VBM, which is agree well with the previous study of Saparov et al. [21].

In the energy range between 2.0 eV and 4.5 eV, there exists a strong hybridization between Sb-d and K-s, Cd-s and Cd-p and also between Sr-p and Sb-d states. In the upper valence band there exists strong hybridization between Sr-s and Sr-p, whereas between Cd-d and Sb-s in the lower valence band.

3.3. Effective mass

We have calculated the effective mass of electrons (m_e^*) from the band structure, the values of the effective mass of electrons are predictable from the curvature of the conduction band minimum. The diagonal elements of the effective mass tensor, m_e, for the electrons in the conduction band are calculated in $R \rightarrow X$ direction in k space using the following well-known relation:

$$\frac{1}{m_e^*} = \frac{1\partial^2 E(k)}{\hbar^2 \partial k^2} \tag{3}$$

The effective mass of electron is determined by fitting the electronic band structure to a parabolic function Eq. (3) in the first Brillouin zone using EVGGA approach. The effective mass of electron for the (symmetry) is obtained from the curvature of the conduction band at $R \rightarrow X$ point. The calculated electron effective mass ratio (m_e^*/m_e) for $K_2SrCdSb_2$ and $K_2BaCdSb_2$ in $R \rightarrow X$ direction is 0.0578 and 0.0433. It is obvious that the calculated value of $K_2SrCdSb_2$ is larger than $K_2BaCdSb_2$ values. Because that the parabolic curvature of $K_2BaCdSb_2$ is greater than $K_2SrCdSb_2$, so we know that the effective mass is inversely proportional to the curvature. We also have calculated the effective mass of the heavy holes and light holes. The calculated values for heavy holes and light holes for $K_2SrCdSb_2$ ($K_2BaCdSb_2$) compounds are 0.02291 and 0.00614 (0.0146 and 0.00618).

3.4. Optical properties

Deep insight into the electronic structures can be achieved by investigating the optical spectra which not only give information about the occupied and unoccupied states, but also about the

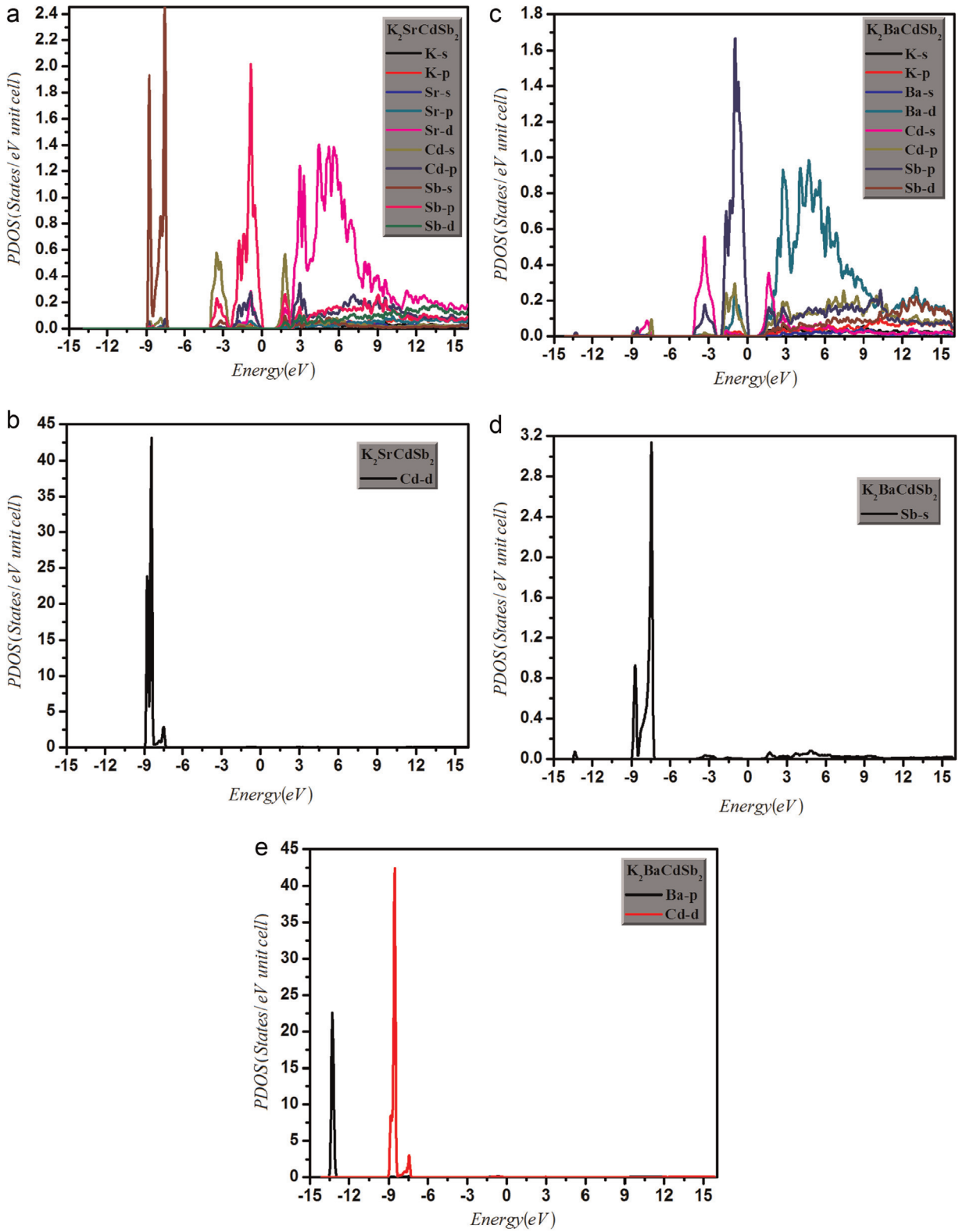

Fig. 5. Calculated band structures for $K_2SrCdSb_2$ and $K_2BaCdSb_2$ compounds.

feature of the bands. Thus we intended to investigate the optical properties of $K_2SrCdSb_2$ and $K_2BaCdSb_2$ compounds. In solid the optical properties are stated by dielectric tensor. The investigated compounds have orthorhombic symmetry, which has three non-zero components $\varepsilon_2^{xx}(\omega)$, $\varepsilon_2^{yy}(\omega)$ and $\varepsilon_2^{zz}(\omega)$ of the second-order dielectric tensor. These components correspond to an electric field parallel and perpendicular and to the *c*-axis. We have calculated the average value of the real $\varepsilon_1(\omega)$ and imaginary $\varepsilon_2(\omega)$ parts of the optical dielectric functions for $K_2SrCdSb_2$ and $K_2BaCdSb_2$ compounds seeking the influence of using different exchange and correlation potentials (LDA, GGA, and EVGGA) on the optical properties (see Fig. 6). The highest spectral peak of the average value of the imaginary part $\varepsilon_2(\omega)$ for $K_2SrCdSb_2$ compound using LDA, GGA and EVGGA are situated at 3.5, 3.7 and 4.0 eV, while for

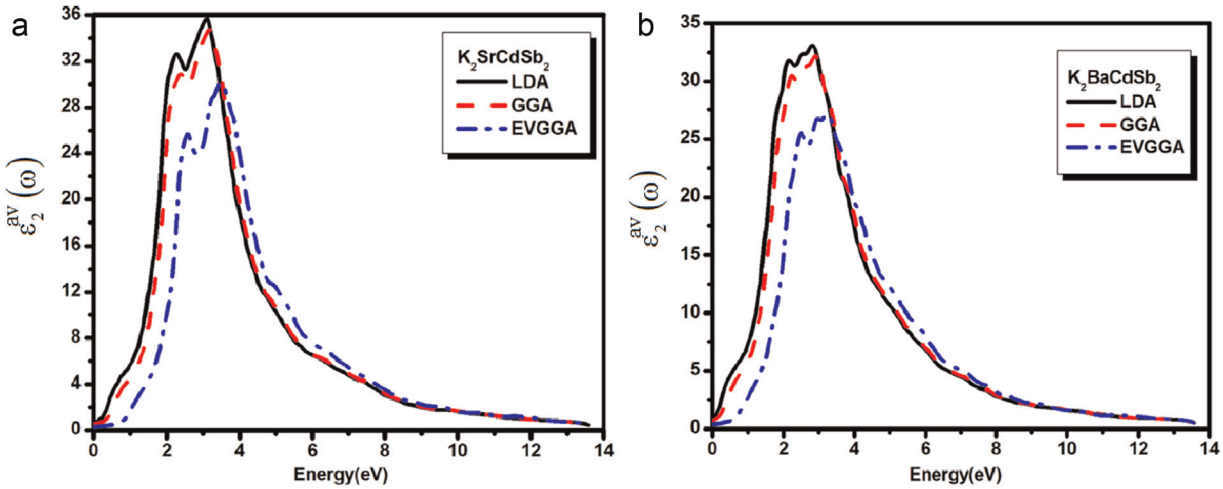

Fig. 6. Calculated average imaginary part of dielectric optical tensor function for K_2SrCdSb2/Ba compounds using LDA, GGA, and EVGGA.

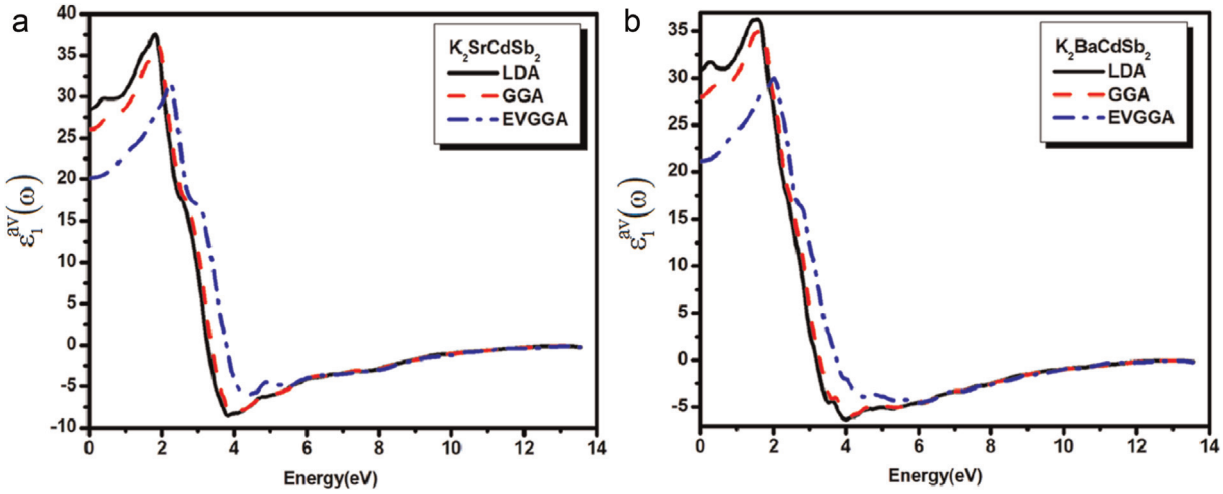

Fig. 7. Calculated average real part of dielectric optical tensor function for K_2SrCdSb2/Ba compounds using LDA, GGA, and EVGGA.

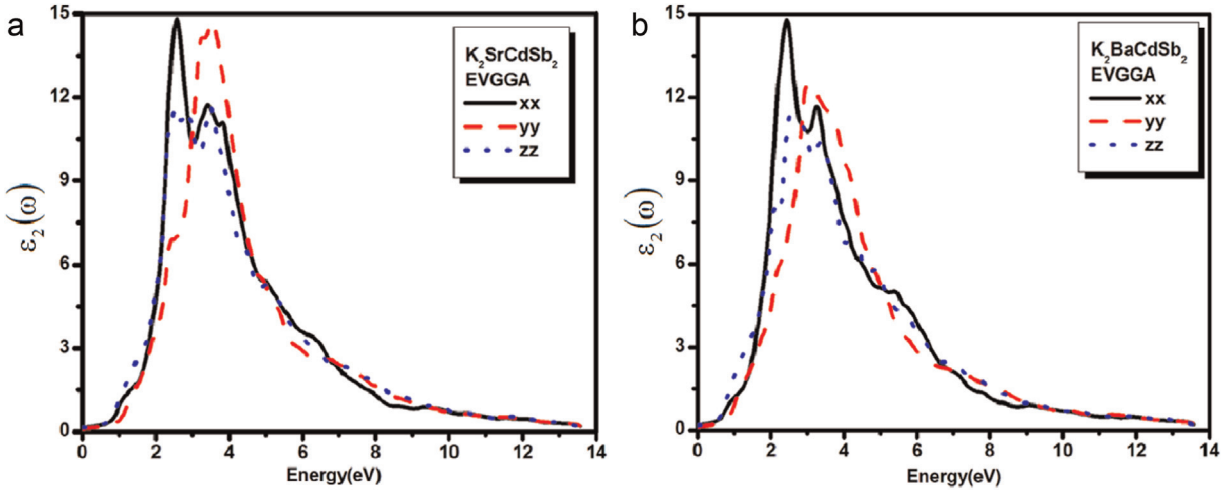

Fig. 8. Calculated $\varepsilon_2^{xx}(\omega)$, $\varepsilon_2^{yy}(\omega)$ and $\varepsilon_2^{zz}(\omega)$ for K_2SrCdSb2/Ba compounds.

$K_2BaCdSb_2$ compound are located at 3.0, 3.2 and 4.0 eV. From the imaginary part $\varepsilon_2(\omega)$, the real part $\varepsilon_1(\omega)$ was also calculated for both compounds by using the Kramers–Kronig equation. The average value of the real part is shown in Fig. 7. The principle peaks of the real part of $K_2SrCdSb_2$ compound are located at 2.0, 2.2 and 3 eV whereas at 2.0, 2.2 and 2.8 eV for $K_2BaCdSb_2$ compound using LDA, GGA and EVGGA, respectively. The calculated values of $\varepsilon_1^{average-LDA}(0)$, $\varepsilon_1^{average-GGA}(0)$ and $\varepsilon_1^{average-EVGGA}(0)$ are 27.0, 22.0 and 20.0 for $K_2SrCdSb_2$ compound while these values are 32.0, 26.0 and 22.0 for $K_2BaCdSb_2$ compound.

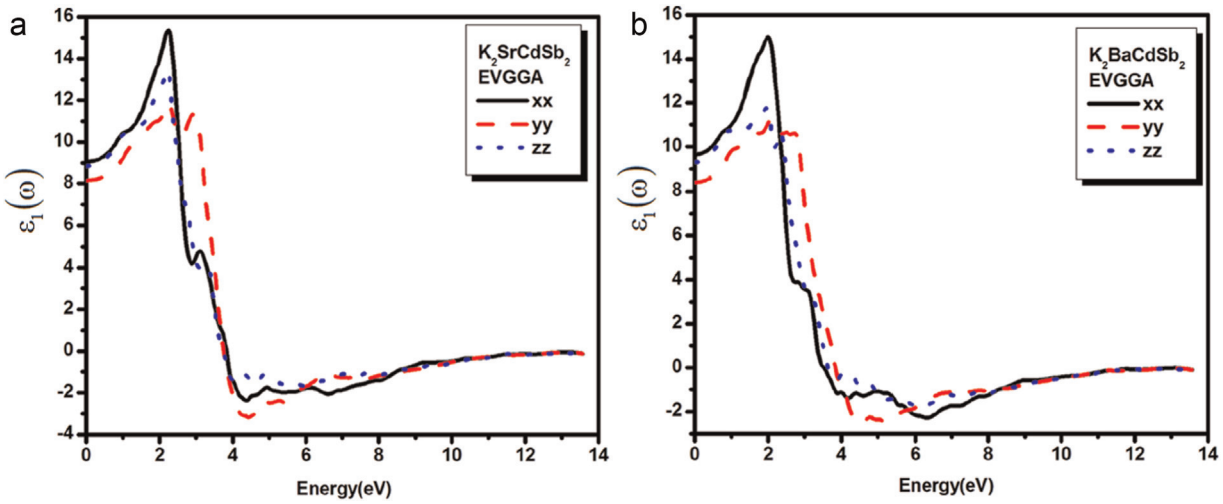

Fig. 9. Calculated $\varepsilon_1^{xx}(\omega)$, $\varepsilon_1^{yy}(\omega)$ and $\varepsilon_1^{zz}(\omega)$ for $K_2SrCdSb2/Ba$ compounds.

Following Figs. 6 and 7 one can see that spectrum is shifted towards higher energies when we move from LDA→GGA→EVGGA with increasing amplitude especially for the first spectral structure at lower energies. It is clear that EVGGA gives advances to a better band splitting and hence better optical gap. Therefore we have selected to show the calculated $\varepsilon_2^{xx}(\omega)$, $\varepsilon_2^{yy}(\omega)$ and $\varepsilon_2^{zz}(\omega)$ spectrum using EVGGA.

Figs. 8 and 9, show the spectrum of the real and imaginary parts of the complex dielectric function versus the photon energy. Our analysis for the $\varepsilon_2^{xx}(\omega)$, $\varepsilon_2^{yy}(\omega)$ and $\varepsilon_2^{zz}(\omega)$ spectrum (Fig. 8) shows that the first critical point (the fundamental absorption edge) of the dielectric function occurs at a round 0.3 eV for $K_2SrCdSb_2$ compound and at 0.5 eV for $K_2BaCdSb_2$ compound. The critical point is occurred at $\Gamma_v - \Gamma_c$, which gives the threshold for the optical transitions between the VBM and the CBM. Beyond this threshold energy (first critical point), the curve increases rapidly. This is due to the fact that the number of points contributing towards $\varepsilon_2(\omega)$ is increased abruptly. The main peak of $\varepsilon_2^{xx}(\omega)$, $\varepsilon_2^{yy}(\omega)$ and $\varepsilon_2^{zz}(\omega)$ spectrum are situated between 2.0 and 4.0 eV. From Fig. 9, it can be seen that at the low-energy region the real part of the dielectric constant increases with energy, and reach its first peak for $\varepsilon_1^{xx}(\omega)$ and $\varepsilon_1^{zz}(\omega)$ at 2.2 eV, while for $\varepsilon_1^{yy}(\omega)$ occurs at 3.0 eV, for $K_2SrCdSb_2$ compound. Whereas for $K_2BaCdSb_2$ compound the peaks for the three components are located at around 3.0 eV.

Beyond 3.0 eV the spectrum of $\varepsilon_1^{xx}(\omega)$, $\varepsilon_1^{yy}(\omega)$ and $\varepsilon_1^{zz}(\omega)$ for both compounds are decreasing and crossing the zero to reach the negative values. The region below the zero shows the reflectivity i.e. this region shows the metallic behavior of the material and the region above from the zero shows the transmission of the light. The calculated values of $\varepsilon_1^{xx}(0)$, $\varepsilon_1^{yy}(0)$ and $\varepsilon_1^{zz}(0)$ are 9.1 (9.5), 9.0 (9.2), 8.0 (8.4) for $K_2SrCdSb_2$ ($K_2BaCdSb_2$) compounds.

4. Conclusion

In this work we reports theoretical study on the structural, electronic and optical properties of $K_2SrCdSb_2$ and $K_2BaCdSb_2$ compounds using FP-LAPW method within LDA, GGA and EV-GGA schemes. The calculation of the electronic properties explore the features of the band structure of the investigated compounds. The compounds possess a direct band gap at the Γ-point of the Brillouin zone of about 0.344 /0.20 eV (LDA), 0.463/0.285 eV (GGA) and 0.904/0.707 eV (EV-GGA) for $K_2SrCdSb_2$ / $K_2BaCdSb_2$. The calculation show that the effective mass of $K_2SrCdSb_2$ is larger than that of $K_2BaCdSb_2$, that is attributed to the fact that the parabolic curvature of $K_2BaCdSb_2$ is greater than that of $K_2SrCdSb_2$, the effective mass is inversely proportional to the curvature. In order to predict the chemical bonding and also the charge transfer in $K_2SrCdSb_2$ and $K_2BaCdSb_2$ compounds, we calculated the charge densities in the (200) crystallographic plane. In addition we have calculated the dielectric optical tensor components of the $K_2SrCdSb_2$ and $K_2BaCdSb_2$ compounds to seek deep insight into the electronic structure.

Aknowledegment

The result was developed within the CENTEM Project, reg. no. CZ.1.05/2.1.00/03.0088, co-funded by the ERDF as part of the Ministry of Education, Youth and Sports OP RDI program. MetaCentrum and the CERIT-SC under the program Center CERIT Scientific Cloud reg. no. CZ.1.05/3.2.00/08.0144.

References

[1] Y. Kamihara, T. Watanabe, M. Hirano, H. Hosono, Iron-based layered superconductor La[$O_{1-x}F_x$]FeAs (x=0.05-0.12) with T_c=26K, J. Am. Chem. Soc. 130 (2008) 3296–3297.
[2] J.H. Tapp, Z. Tang, B. Lv, K. Sasmal, B. Lorenz, P.C.W. Chu, A.M. Guloy, Phys. Rev. B 78 (2008) 060505R.
[3] Shawna R. Brown, Susan M. Kauzlarich, Franck Gascoin, G. Jeffrey Snyder, Yb14MnSb11: new high efficiency thermoelectric material for power generation, Chem. Mater. 18 (2006) 1873.
[4] M. Rotter, M. Tegel, D. Johrendt, Phys. Rev. Lett. 101 (2008) 107006.
[5] K. Sasmal, B. Lv, B. Lorenz, A. Guloy, F. Chen, Y.-Y. Xue, C.-W. Chu, Phys. Rev. Lett. 101 (2008) 107007.
[6] J.-T. Han, J.-S. Zhou, J.-G. Cheng, J.B. Goodenough, J. Am. Chem. Soc. 132 (2010) 908.
[7] F. Gascoin, S. Ottensmann, D. Stark, S.M. Haïle, G.J. Snyder, Adv. Funct. Mater. 15 (2005) 1860.
[8] H. Zhang, J.T. Zhao, Yu Grin, X.J. Wang, M.B. Tang, Z.Y. Man, H.H. Chen, X. X. Yang, J. Chem. Phys. 129 (2008) 164713.
[9] E.S. Toberer, A.F. May, B.C. Melot, E. Flage-Larsen, G.J. Snyder, Dalton Trans. 39 (2010) 1046.
[10] G.J. Snyder, E.S. Toberer, Nat. Mater. 7 (2008) 105.
[11] B. Saparov, S.-Q. Xia, S. Bobev, Inorg. Chem. 47 (2008) 11237.
[12] B. Saparov, H. He, X.H. Zhang, R. Greene, S. Bobev, Dalton Trans. 39 (2010) 1063.
[13] S.-Q. Xia, S. Bobev, Inorg. Chem. 46 (2008) 874.
[14] S.-Q. Xia, S. Bobev, Inorg. Chem. 47 (2008) 1919.
[15] B. Saparov, S. Bobev, Inorg. Chem. 49 (2010) 5173.
[16] B. Saparov, S. Bobev, A. Ozbay, E.R. Nowak, J. Solid State Chem. 181 (2008) 2690.
[17] S.-Q. Xia, S. Bobev, J. Comput. Chem. 29 (2008) 2125.
[18] S.-Q. Xia, S. Bobev, J. Am. Chem. Soc. 129 (2007) 10011.
[19] B. Saparov, M. Broda, K.V. Ramanujachary, S. Bobev, Polyhedron 29 (2010) 456.

[20] L. Pauling, The Nature of the Chemical Bond, Cornell University Press, Ithaca, NY, 1960.
[21] B. Saparov, M. Saito, S. Bobev, J. Solid State Chem. 184 (2011) 432–440.
[22] P. Blaha, K. Schwarz, J. Luitz, WIEN97: A Full Potential Linearized Augmented Plane Wave Package for Calculating Crystal Properties, Techn. Universitat Wien, Austria, 1999 (ISBN:3-9501031-0-4).
[23] P. Hohenberg, W. Kohn, Phys. Rev. 136 (1964) B864.
[24] D.M. Ceperley, B.J. Alder, Ground state of the electron gas by a stochastic method, Phys. Rev. Lett. 45 (1980) 566–569.
[25] J.P. Perdew, K. Burke, M. Ernzerhof, Phys. Rev. Lett. 77 (1996) 3865.
[26] E. Engel, S.H. Vosko, Phys. Rev. B 50 (1994) 10498.
[27] A. Delin, P. Ravindran, O. Eriksson, J.M. Wills, Int. J. Quantum Chem. 69 (1998) 349.
[28] W.T. Ching, P. Rulis, Phy. Rev. B 73 (2006) 045202.
[29] F.D. Murnaghan, Proc. Natl. Acad. Sci. USA 30 (1944) 244.